

# Understanding mechanisms of JAK1 inhibition on synovial fibroblasts using combinatorial approaches of bulk and single cell RNAseq analyses

Y. Son, D. Korenfeld, A. Suarez-Fueyo, M. Ruzek, J. Wang, B. Harvey

AbbVie Bioresearch Center, Worcester, MA, USA.

---

## Abstract

### Objective

*The aim of these studies was to characterise the molecular effects of a tool JAK1 inhibitor on cultured primary fibroblast-like synoviocytes (FLS) from patients with rheumatoid arthritis (RA) through both total and individual cell analysis.*

---

### Methods

*RA-FLS cultures from 6 (Bulk RNA-seq) or 4 (ScRNA-seq) donors were pre-treated with various concentrations (100 nM and 1µM) of ABT-317 with/without exposure to 25% SEB-conditioned PBMC medium to mimic the RA inflammatory milieu. Cells were subjected to both bulk RNA-seq (36 libraries) and single cell RNA-seq (scRNA-seq; 24 libraries) to identify biological processes impacted by CM and ABT-317 treatments.*

---

### Results

*In our bulk RNA-seq analysis, a total of 2,605 differentially expressed genes (DEGs) were identified between CM-stimulation and unstimulated groups, while 1,122 DEGs were found between ABT-317 1µM and DMSO in CM-stimulated groups using thresholds of  $\log_2$  (fold change)  $\geq 10.581$  and  $FDR \leq 10\%$ . Both bulk and single cell mRNA analysis of RA-FLS treated with a combination of CM and ABT-317 demonstrated the expected changes in inflammatory pathways such as interferon and IL-6 signalling. However, other non-inflammation associated pathways were also altered by ABT-317. In addition, the single cell analysis highlighted that FLS segregate into distinctive clusters upon combination CM and ABT-317 treatment, suggesting JAK inhibition can drive RA-FLS into multiple heterogenous cell populations. Interestingly, one of the unique RA-FLS clusters that emerged from the CM and ABT-317 treatment showed matrix metalloproteinase-3 (MMP3)<sup>high</sup> expression as well as several gene signatures that are not found in any other ABT-317 derived clusters.*

---

### Conclusion

*JAK inhibition with ABT-317 is effective at globally inhibiting CM-induced pro- and non-inflammatory pathways in FLS cultures, but also results in several distinct fibroblast populations with unique gene-associated pathways. This study advances the molecular understanding of JAK1 inhibitor effects on fibroblasts that may contribute to clinical efficacy.*

---

### Key words

JAK1 inhibitor, rheumatoid arthritis, fibroblast, FLS, scRNAseq

Yuna Son, PhD  
 Daniel Korenfeld, BS  
 Abel Suarez-Fueyo, PhD  
 Melanie Ruzek, PhD  
 Jing Wang, PhD  
 Bohdan Harvey, PhD

Please address correspondence to:

Yuna Son  
 AbbVie Bioresearch Center,  
 100 Research Drive,  
 Worcester, MA 01605, USA.  
 E-mail: [sonyuna90@gmail.com](mailto:sonyuna90@gmail.com)

Received on January 9, 2024; accepted in revised form on April 29, 2024.

© Copyright CLINICAL AND EXPERIMENTAL RHEUMATOLOGY 2024.

## Introduction

Rheumatoid arthritis (RA) is an autoimmune disease that is characterised by inflammation of synovium, cartilage destruction, and bone erosion (1). While current therapies for RA have significantly improved the quality of life for RA patients, achieving and maintaining long-term remission of RA is still challenging (2). The Janus Kinase (JAK)-signal transducer and activator of transcription (STAT) signalling pathway plays an important role in human immune response including immune fitness, tissue repair, inflammation, apoptosis, and adipogenesis (3). There are 4 different JAKs which associate with 7 distinct STATs in mammals, and the activation of the JAK-STAT pathway induces a tightly controlled, multiple components, signalling cascade. The JAK-STAT signalling pathway is also closely linked with inflammatory and autoimmune diseases (4) and has led to the therapeutic development of JAK inhibitors (JAKi) for clinical use in several autoimmune diseases, including RA. While the mechanism of action of JAK inhibitors on immune cells in RA patients has been extensively studied and reviewed (5) synovial fibroblasts are also emerging as a key target cell type for JAK inhibitors. Previous studies have shown that FLS can contribute to RA pathogenesis due to their increased invasiveness and production of factors that promote joint damage (6). The JAK-STAT signalling pathway is known to be activated in FLS upon exposure to the inflammatory stimulation such as RA synovial fluid or pro-inflammatory cytokines (4). The JAK-STAT signalling-mediated cytokines can facilitate the recruitment of macrophages, T cells, B cells and dendritic cells and it helps to maintain and promote synovial inflammation (7). These data indicate that the JAK-STAT associated crosstalk between FLS and immune cells might be a prominent driver of RA synovial pathogenesis. Single-cell RNA sequencing of RA synovial tissue has revealed a heterogeneous population of synovial fibroblasts (8-10) that may be related to functional activities in disease (9, 10). For example, THY1<sup>+</sup>CD34<sup>+</sup>HLA-DRA<sup>hi</sup> fibro-

blasts expressed genes related to MHC class II presentation and the interferon gamma-mediated signalling pathway while other fibroblast subpopulations expressed genes involved in matrix remodelling (9). Given this heterogeneity in gene expression and function of synovial fibroblasts, the impact of JAK inhibitors could be varied.

Because the mechanism of action of JAK inhibitors on pathogenic features of FLS has not been extensively studied we aimed to explore the transcriptional changes induced in RA-FLS cells following stimulation with Staphylococcus enterotoxin B (SEB)-conditioned PBMC medium (CM) and the tool JAK inhibitor, ABT-317. We used a combination of bulk and single-cell RNA sequencing (scRNA-seq) approaches to better understand the impacts of JAK1 inhibition at the population and single cell level. Herein, to our knowledge we have provided the first global transcriptomic analysis of the effects of SEB- conditioned PBMC medium and JAK1 inhibitor on human RA-FLS cells. This study explored JAK inhibition mechanism especially involved in RA fibroblast pathogenesis and suggested further research to understand the heterogenous cell status changes in RA-FLS after JAKi treatment, thus advances our understanding of JAK inhibitors and how they may contribute to clinical efficacy.

## Methods

### Culture of human fibroblast-like synoviocyte (FLS)

Human RA FLS were commercially obtained from 6 established RA patients (commercially purchased from Articular Engineering). Cells were cultured in synoviocyte growth medium (Cell Application, Inc.) at 37°C in a 5% of carbon dioxide humidified incubator. Cells were sub-cultured when the culture reached 70-80% confluence and harvested for use in experiments at low passage (Passage 3). Cells were pre-treated with either the vehicle Dimethyl sulfoxide (DMSO) or 100nM and 1µM of ABT-317 (the JAK1 selective inhibitor, provided by AbbVie Bioresearch Center, dose was determined by previous research (11)) for 1hr followed by

### Competing interests:

Y. Son and D. Koenfeld are Abbvie employees; M. Ruzek is an Abbvie employee/ retiree and stockholder; A. Suarez-Fueyo, J. Wang and B. Harvey are Abbvie employees and stockholders. The design, study conduct, and financial support for this research were provided by AbbVie. AbbVie participated in the interpretation of data, review, and approval of the publication.

culture media or Staphylococcal enterotoxin B-stimulated human PBMC (Commercially purchased from Biological Specialty Corporation) (25% of total volume) (CM-stimulation) to replicate the inflammatory milieu in the RA synovium. CM-stimulation induces pro-inflammatory cytokines, tumor necrosis factor  $\alpha$  (TNF- $\alpha$ ), interleukin 1 (IL-1) and gamma interferon (IFN $\gamma$ ) that can contribute to the activation of the JAK-STAT signalling pathway (12). The plates were returned to the incubator at 37°C for a 24-hour period. FLS that were used for these studies are listed in Table I.

#### Cell cytotoxicity assay

Human FLS were seeded in 12-well plates cultured upon reaching 70-80% confluence. Cells were harvested as described above. Cell viability was assessed with the Cell Titer-Glo Luminescent Cell Viability Assay (Promega Corp). Lysis reaction was carried on an orbital shaker for 2 minutes and 80  $\mu$ L of cell lysates from each well were transferred to Costar black 96-well plates (Corning, 3603). Samples were analysed in triplicate for overall luminescence signals using the Envision (Perkin Elmer).

#### RNA extraction

Total RNA was isolated from FLS by RNeasy Micro Kit with DNase treatment (Qiagen) after being treated in the same manner as described above. The quality and quantity of each RNA sample was measured by TapeStation (Agilent).

#### Quantitative reverse transcriptase real time PCR (qRT-PCR)

cDNA was generated from 300 ng of total RNA by reverse transcription with High-Capacity cDNA kit (Applied Bioscience, 4368813). Quantitative PCR (qPCR) was performed on QuantStudio 7-Flex (ThermoFisher) using Taqman Fast Advanced Master Mix (Applied Bioscience, 4444557) with six biological replicates (2 technical replicates). The cycle threshold (Ct) values of genes were normalised to the Ct value of GAPDH in the same sample. The data analysis was performed by  $2^{-\Delta\Delta Ct}$  meth-

**Table I.** RA sample information.

Donors	Type	Cytotoxicity	Bulk RNA-seq	qRT-PCR	Single-cell RNA-seq
1462	RA	X	X	X	
1475	RA	X	X	X	X
1481	RA	X	X	X	
1499	RA	X	X	X	X
2956	RA	X	X	X	X
87554A1	RA	X	X	X	X

6 RA patient samples were used for bulk RNA-seq, cell cytotoxicity test, and qRT-PCR.

4 RA patient samples were used for scRNA-seq.

od. Primer information for qRT-PCR is shown below (Supplementary Table 7).

#### RNA-seq

250 ng of total RNAs were used for library preparation for RNA-seq. NEB-Next Ultra™ Directional RNA Library Prep Kit for Illumina (NEB, E7420) and NEBNext Poly(A) mRNA Magnetic Isolation Module (NEB, E7490) were used for library preparation. The RNA-seq libraries were sequenced on a NovaSeq 6000 sequencer (Illumina) to obtain 2 x 150-base pair reads performed in 36 samples. The estimated coverage was around 30 million reads per sample.

#### RNA-seq analysis

The raw data were trimmed with Trim-Galore and Cutadapt. FASTQC was used to filter out reads of low to moderate quality. Paired-end reads were mapped to the GRCh38 reference genome using Salmon. EdgeR, limma-voom, and 3D RNA-seq R package were used to identify differentially expressed genes (DEGs) at both log fold change ( $\log_{2}FC \geq 10.581$ ) and a 10% false discovery rate (FDR) using the Benjamini-Hochberg procedure to adjust P values. FDR 10% threshold was used for further analyses to capture the JAK1 inhibition signals due to the artificial stimulatory conditions created by CM (25%) stimulation. Batch effects of biological replicates were removed from the data using the RUVSeq method (13). Annotation of the genes and pathways was provided by the Gene Set Enrichment Analysis (GSEA), Molecular Signatures Database (MSigDB). Gene Expression Omnibus (GEO) repository data sets (GSE12021 (14) and

GSE55457 (15)) from RA synovial tissue studies were used to compare with this study. DEGs were identified in the tissue data with limma R package using the same thresholds with other data.

#### Single-cell RNA sequencing using 10X genomics platform

To enable to observe phenotypic heterogeneity of FLS, four donors were selected in early passage (under passage 3) for scRNAseq. Human FLS were harvested and stained with CalceinAM Viability dye (ThermoFisher), CellTrace Violet (ThermoFisher), CellTrace Yellow (ThermoFisher), TotalSeq-B anti-human Hashtag antibodies (Biolegend, Suppl. Table S8). Viable cells were sorted using a BD FACSAria Fusion cell sorter. Each donor sample was pooled and loaded together onto a single lane of the 10x Chromium Single Cell Chip using CellTrace dyes and TotalSeq-B anti-human Hashtag antibodies (Biolegend). Then, 65,000 cells per sample were super-loaded into a 10X Chromium controller, and library preparation was performed according to the manufacturer's protocol using Chromium Single Cell 3' Library & Gel Bead Kit v. 3.2 (10X Genomics). The resulting libraries were sequenced in an Illumina Nextseq2000 sequencer according to 10X Genomics recommendation to a depth of around ~11-15,000 reads per cell.

#### Single-cell RNA sequencing data analysis

Count matrices were generated from fastq files using the Cellranger version 6.1.2 count pipeline against the GRCh38 genome. Total 87,108 cells were recovered and scRNA-seq down-

stream analysis was performed with Seurat version 4 package in R (16). Low quality cells were removed by filtering out cells for which fewer than 200 genes or higher than 3,500 genes. Also, Cells with greater than 10% of mitochondrial RNA content were removed. Multiplexed samples were demultiplexed using HTODemux method with the default settings. Doublet cells were identified by hashtag antibodies and removed by the HTODemux function. Then, the UMI count matrices were normalised using the SCTransform method (17) with the number of reads, percentage mitochondrial reads, S phase cell cycle score and G2M cell cycle phase score. Harmony R package was used to correct the batch effect of conditioned media stimulation and donors. The first 20 principal components (PCs) were used to reduce the dimensionality of the dataset, and the PCs were used for Seurat's RunUMAP and FindNeighbors analyses. We identified the cell clusters using the Seurat's FindClusters function with a resolution of 0.2. Differentially expressed genes (DEGs) were identified by Seurat's FindAllMarkers. DEGs between different treatments were identified with pseudobulk DESeq2. Hallmark gene set enrichment scores are calculated across clusters using the R package singleseqset (18). In brief, the package used a modified version of the competitive gene set enrichment test CAMERA by calculating variance inflated Wilcoxon rank sum testing. Differentially expressed genes between two clusters were identified by Seurat's Findmarkers function. In brief, we used top 20 marker genes using Harmony from the study and enrich the gene signatures using singleseqset R package. Singleseqset results were plotted with a threshold of FDR <10%.

#### Statistical analysis

The significance of the difference between the groups was statistically analysed by Wilcoxon Rank Sum test unless otherwise mentioned. *p*-values from relative cell proliferation measurement were calculated using an unpaired Wilcoxon rank sum test and adjusted for multiple testing with the Holm-Bon-

ferroni method. Venn-diagram overlaps were tested with Fisher's exact test.

#### Results

##### *ABT-317 reverses the effects of CM-stimulation on RA-FLS cells*

To investigate the impact of JAK inhibition on the pathogenic features of the FLS, we established an *in vitro* model with primary human RA-FLS with and without stimulation with Staphylococcus enterotoxin B (SEB)-conditioned PBMC medium (CM) to mimic the inflammatory milieu in the RA synovium. We tested if ABT-317, a tool JAK1 selective inhibitor, could reverse the effects of CM-stimulation on RA-FLS cells. As shown in Fig. 1A and Table I, six different RA patient derived-FLS cells were pre-treated with DMSO (vehicle for JAKi) or ABT-317 (0.1µM, 1µM) for 1hr before combining with culture media or 25% of total volume of conditioned media (CM) for 24 hrs. Cell viability following all CM, ABT-317 or combination was minimally impacted (Suppl. Fig. S1).

Given that limited cytotoxicity was observed with either CM stimulation or ABT-317 exposure, we proceeded to extract RNA for cDNA library generation and next-generation sequencing to create the transcriptomic profile for each of the treatment conditions. Then, we examined global gene expression changes triggered by CM-stimulation and ABT-317 treatment using principal component analysis (PCA) (Fig. 1B). Interestingly, ABT-317 treatment alone did not have a significant impact on the global gene expression changes, while ABT-317 in combination with CM showed distinct global gene expression differences in a dose dependent manner as observed in PC1 (Fig. 1B. DMSO vs. ABT-317 1µM (CM-Stim): *p*=0.02). Based on these findings, we used only ABT-317 1µM samples for downstream analyses as the low dose group did not show strong effects on RA-FLS cells. From the RNA-seq analysis, a total of 2,605 differentially expressed genes (DEGs) were identified between CM-stimulation and unstimulated groups, while 1,122 DEGs were found between ABT-317 1µM and DMSO in CM-stimulated groups using thresholds

of  $\log_2(\text{fold change}) \geq |0.58|$  and FDR  $\leq 10\%$  (Fig. 1C, Suppl. Table S1). We found a significant overlap ( $p < 2.22e^{-16}$ ) in the genes perturbed by CM-stimulation and by the addition of ABT-317 in opposite directions (Fig. 1D), indicating that JAKi reverses CM-stimulated effects.

Next, we determined if the RA-FLS cells with CM-stimulation can reflect similar gene expression changes of an inflamed RA synovial tissue. We measured the correlations between public RA tissue microarray dataset (GSE12021: RA vs. Normal and RA vs. OA (14); GSE55457: RA vs. OA (15)) and our bulk RNA-seq data (Fig. 1E). We observed significant correlations between RA-FLS dataset and DEGs (RA and OA) from GSE12021 ( $R=0.46$ ,  $p=6.79e^{-7}$ ) and between RA-FLS dataset and DEGs (RA and OA) from GSE55457 ( $R=0.4$ ,  $p=1.98e^{-6}$ ). We also compared the DEGs (RA and normal) from GSE12021 with our RA-FLS dataset with similar results. These results indicated that our CM-stimulated RA-FLS cells reflects some of the same pathways within inflamed synovium, although limited by the *in vitro* cell monoculture conditions.

##### *ABT-317 affects immune and non-immune related pathways*

We used Hallmark gene sets from Molecular Signatures Database (MSigDB) to understand representative well-defined biological pathways in this study. Gene set enrichment analysis (GSEA) using Hallmark gene sets demonstrated that ABT-317 reverses CM-stimulation induced pathways (Fig. 2A and B). CM-stimulation increases both IL6-JAK-STAT3 and interferon (IFN) signalling pathways that drive inflammation while these same inflammation related pathways are dampened by JAK inhibition with ABT-317 (Fig. 2A). These findings were the expected impact of CM-stimulation and JAK inhibition with ABT-317 on the FLS. Similarly expected, ABT-317 impacted the IL6-JAK-STAT3 pathways by decreasing levels of IL18R1, MYD88, STAT3, and TLR2 (Fig. 2C, Suppl. Tables S2 and 3). Also, we did see a reduction in IRF1, IDO1, and HIF1A expression level (Fig. 2D,

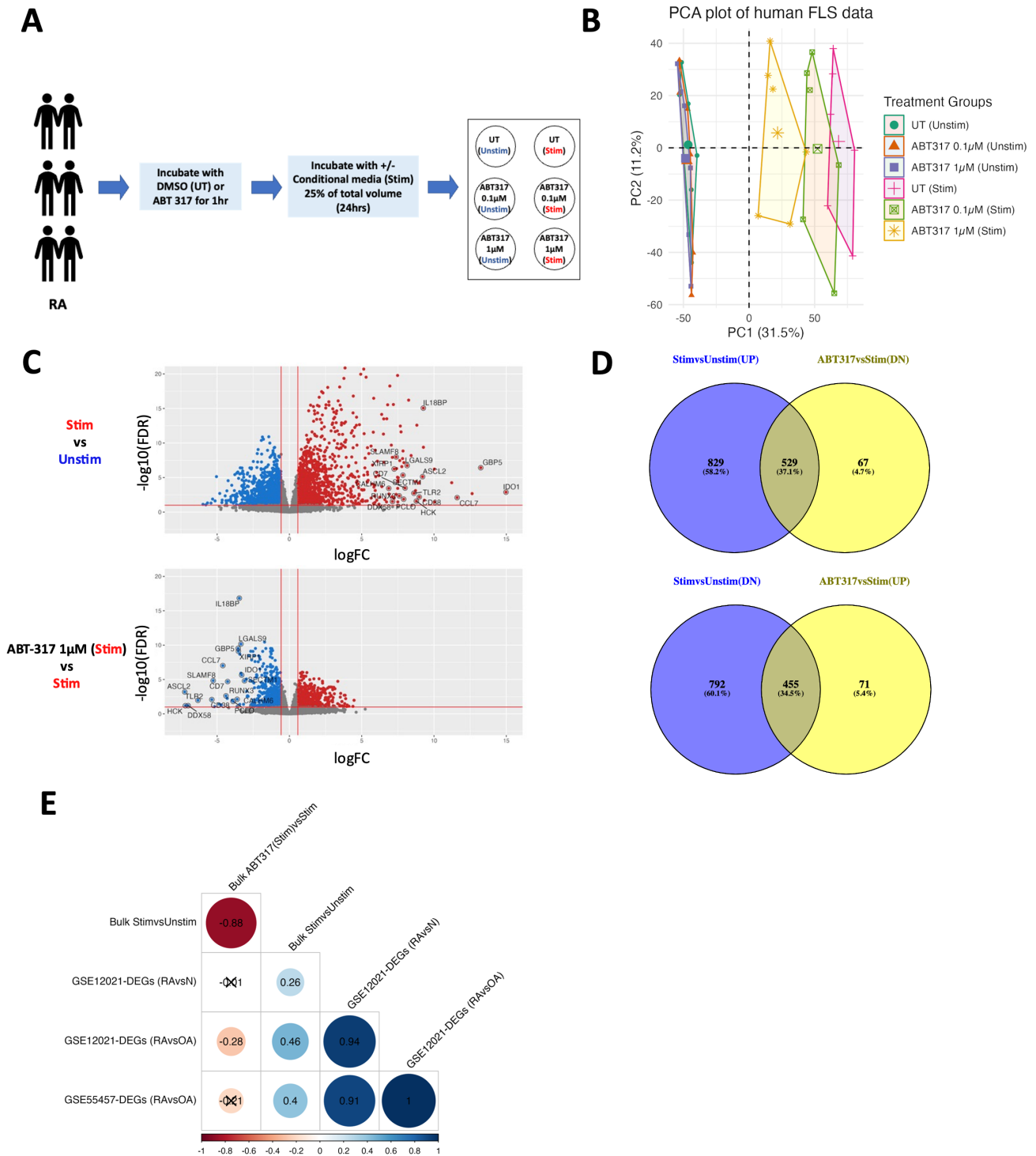


**Fig. 1.** ABT-317 reverses the effects of CM-stimulation on RA-FLS cells.

**A:** RA patient-derived cells were incubated with DMSO (UT) or ABT-317 for 1 hr. Treated cells were incubated with and without conditioned media stimulation (25% of total volume) for 24 hrs. Cells were harvested and used for further experiments.

**B:** Principal component analysis (PCA) plot showing the distribution of conditioned media (Stim) and ABT-317 treatment samples. The differences along PC1 between groups were measured with Wilcoxon rank sum test (ABT-317 1µM (Stim) vs. Stim;  $p=0.02$ ).

**C:** (Up) Volcano plot demonstrating the significantly increased RNA expression levels in samples with conditioned media (Stim). (Down) Volcano plot showing the significantly decreased RNA expression levels in samples after treating ABT-317 1µM (Stim). Red dots and blue dots represent the significantly upregulated and downregulated genes respectively with a foldchange (FC) ( $|\log_2(\text{FC})| \geq 0.58$ , vertical line) and false discovery rate ( $-\log_{10}(\text{FDR}) \leq 0.1$ , horizontal line). Overlapped genes were selected by top overlapped  $\log_2(\text{FC})$  values from each comparison.

**D:** Venn diagrams of differentially expressed genes (DEGs) in Stim vs. Unstim (UP/DN) and ABT-317 1µM (Stim) vs. Stim (DN/UP) showing the number of unique and overlapping DEGs. Overlap of DEGs was tested using Fisher's exact test ( $p < 2.22e^{-16}$ ).

**E:** Correlation heatmap plots for DEGs among synovial tissue datasets (GSE12021 and GSE55457) and bulk RNAseq. Pearson's correlation coefficient values (R) among tissue datasets and bulk RNA seq DEGs results were calculated. Insignificant ( $p > 0.05$ ) value is marked as a cross (X).

Suppl. Tables S2 and 3) suggesting that it is likely ABT-317 affects IFN gamma signalling.

Interestingly, pathways not directly related to inflammatory signalling, such as hypoxia, cell migration, complement, and coagulation are also downregulated by ABT-317. Furthermore, cell cycle pathways are upregulated by JAK inhibition, while stimulation with CM decreases the cell cycle related pathways (Fig. 2B), suggesting that additional pathogenic mechanisms in synovial fibroblasts are also impacted by JAK inhibition. We mainly focused on HIF1A mediated hypoxic stress pathway since HIF1A mediated hypoxia is known to activate cancer-associated fibroblasts (CAFs), and it has been shown to induce epithelial mesenchymal transition (EMT) in prostate cancer cells (19). We have identified that the hypoxia Hallmark gene set was significantly enriched in stimulated FLS while ABT-317 causes a reduction in this signature (Fig. 2A). Interestingly, we found that several genes involving a hypoxic-like response and extracellular matrix (ECM) modification were also impacted by stimulation with CM or ABT-317 treatment. For example, LOX, P4HA1, and P4HA2 were upregulated by CM-stimulation whereas exposure to ABT-317 (CM-stim) reversed this upregulation (Fig. 2E, Suppl. Tables S2 and 3). We have also examined whether the cell migration gene set signature is changed by CM or ABT-317 treatment since multiple reports suggest hypoxia affects cell morphology and behaviour such as cell migration and invasion (20,21). We did find that the cell migration gene set signature was significantly enriched in CM-stimulated FLS while ABT-317 treatment reduced this signature (Fig. 2A and Fig. 2F). Also, ABT-317 reduced the gene expression level of several hypoxia related genes known to be involved in cell migration/invasion such as LOX (22), SLC2A1 (23), PGK1 (24), and PPFIA4 (25) (Suppl. Tables S2 and 3). Given this unique finding we confirmed the similar effects of CM-stimulation and ABT-317 on downstream hypoxia related stress pathways in RA-FLS cells.

#### *qRT-PCR confirmed that ABT-317 may reduce hypoxia-related pathways in RA-FLS cells*

Synovial hypoxia is considered as a potential pathogenic factor in RA due to its ability of inducing pathways like angiogenesis, inflammation, abnormal metabolism, and cartilage erosion (26). To further investigate the impact of ABT317 on hypoxia on RA FLS cells, we selected genes involved in the hypoxic related pathways like angiogenesis (VEGFA), abnormal metabolism (HIF1A, SLC2A1, HK2, PGK1, IL32), ECM modifications (PLOD2, P4HA1, LOX, LOXL3) for additional confirmatory analyses. We performed qRT-PCR analysis from the same donors that were evaluated earlier by RNAseq. Most of the genes detected by qRT-PCR showed similar expression patterns with those identified from RNA seq data ( $R=0.96$  (StimvsUnstim) and  $R=0.94$  (ABT317(Stim)vsStim),  $p<0.001$  from Pearson's correlation) (Fig. 3A, Suppl. Table S4).

We found that HIF1A is upregulated (1.83-fold) following CM-stimulation compared to unstimulated cells indicating that CM-stimulation may trigger a hypoxic-like response in the RA-FLS (Fig. 3B). In contrast, ABT-317 significantly downregulated HIF1A (0.66-fold) likely leading to the subsequent reduction in hypoxia related gene expression since HIF1A is a major contributor for cell adaptation to hypoxic stress (27). Also, we determined CM-stimulation increased the expression of SLC2A1 (3-fold), PGK1 (2.89-fold), HK2 (2.59-fold), and IL32 (188.3-fold) showing that glycolysis is induced by inflammatory stress on RA fibroblasts (Fig. 3C). We also observed significant reduction of glycolysis genes like SLC2A1 (0.38-fold), HK2 (0.54-fold), and PGK1 (0.45-fold) following exposure to ABT-317. Interestingly, we found CM-stimulation greatly increased the gene expression of IL32, and IL32 is known to induce glycolytic activity by increasing lactate dehydrogenase (LDH) activity (28). We observed decreased expression of LDHA after treating with ABT-317 (Stim) in our RNA-seq data (Fig. 2E, Suppl. Table S3) indicating that ABT-317 affects metabolic

process in RA-FLS cells by targeting different glycolytic enzymes. Furthermore, we identified that CM-stimulation increased angiogenesis genes (Fig. 3D) such as VEGFA (1.54-fold) and ECM-modification genes (Fig. 3E) like PLOD2 (5.31-fold), LOXL3 (1.3-fold), and P4HA1 (1.67-fold) whereas exposure to ABT-317 caused a reduction in the expression levels of PLOD2(0.69-fold) and LOX (0.62-fold) genes compared to stimulated cells. This indicates that CM-stimulation triggers not only inflammatory responses but also ECM-modification, metabolic changes, and hypoxia related stress that are effectively reversed by JAK inhibition.

#### *Heterogeneous cell states of RA-FLS cells in single cell RNA sequencing*

According to our bulk RNAseq analysis of RA-FLS, ABT-317 is effective in reducing several of the inflammatory as well non-inflammatory genes/pathways induced by CM-stimulation within the total RA-FLS population. Given that the FLS are primary cell cultures derived from RA patient synovial tissue that have been shown previously to be heterogenous in their phenotype (8-10), we sought to examine the response of our RA-FLS cells to CM-stimulation and ABT-317 exposure at single-cell resolution level using scRNA-seq. RA-FLS cells from four RA donors were cultured with and without CM-stimulation and ABT-317 as described earlier (Fig. 1A and Table I) and subjected to cell sorting for individual cell capture/sequencing by using 10X Genomics technology. After quality filtering, we obtained 87,108 cells, and clustering analysis revealed nine distinct clusters driven by different treatment schemes (Fig. 4A). Clusters 0, 6, and 7 mainly consisted of unstimulated cells with no difference being detected among the CM-stim and ABT-317 treatment groups within each cluster, which was consistent with bulk RNA-seq data (Fig. 1B and Fig. 4B). We then compared single cell RNA-seq to bulk RNA-seq data and observed a high level of correlations between the identified DEGs (StimvsUnstim:  $R=0.96$ , ABT-317 (Stim) vs Stim:  $R=0.95$ , Pearson's correlations  $p<0.05$ )

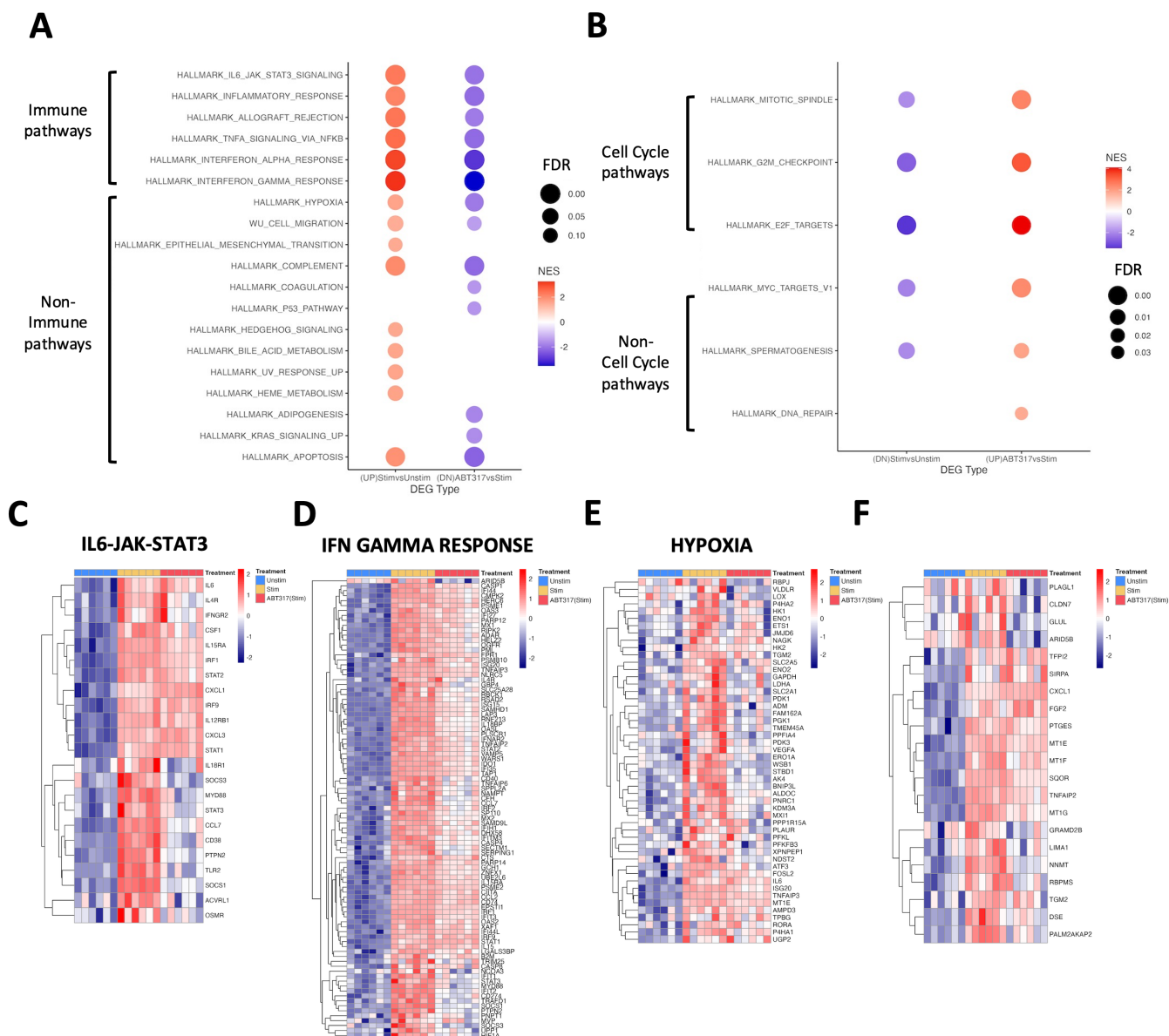


**Fig. 2.** Gene expression patterns of the GSEA enriched signatures. **A:** Gene set enrichment analysis (GSEA) demonstrating the degree of enrichment of the significant hallmark signatures (FDR <15%) in upregulated genes in Stim vs. Unstim (DEGs) and downregulated genes in ABT317 (Stim) vs. Stim (DEGs). NES, normalised enrichment score. **B:** Gene set enrichment analysis (GSEA) demonstrating the degree of enrichment of the significant hallmark signatures (FDR <15%) in downregulated genes in Stim vs. Unstim (DEGs) and upregulated genes in ABT317 (Stim) vs. Stim (DEGs). NES, normalised enrichment score. **C:** Heatmap plot revealing the expression of the genes for Hallmark IL6-JAK-STAT3 signalling signature in RA-FLS cells with different treatment groups. Color scale indicates the relative gene expression. **D:** Heatmap plot revealing the expression of the genes for Hallmark IFN-gamma response signalling signature in RA-FLS cells with different treatment groups. Colour scale indicates the relative gene expression. **E:** Heatmap plot revealing the expression of the genes for Hallmark Hypoxia signature in RA-FLS cells with different treatment groups. Colour scale indicates the relative gene expression. **F:** Heatmap plot revealing the expression of the genes for WU-Cell migration signature in RA-FLS cells with different treatment groups. Colour scale indicates the relative gene expression. WU-Cell migration gene set consists of genes associated with migration rate of 40 human bladder cancer cell lines.

(Fig. 4C). Clusters 0, 6 and 7 largely reflect the unstimulated fibroblasts with or without ABT-317. Clusters 1 and 8 are largely the result of CM-stimulation and clusters 2 and 5 reflect CM + ABT-317 treatment and fall intermediately between stimulated and unstimulated clusters (Fig. 4B). The marker genes for

each cluster were identified (Suppl. Fig. S23 and Suppl. Table S5) and several marker genes are specifically expressed in certain clusters (cluster 3: CHI3L1; cluster 4: PENK and PRG4; cluster 5: MMP3; cluster 6: TRH and FHL1; cluster 7: KRT14 and KRT16; cluster 8: MT1 genes).

To understand the heterogenous cellular response of the RA-FLS cells to ABT-317 treatment, we explored the changes in gene signatures at the single cell resolution level. Each cluster was tested for enrichment scores of human Hallmark gene sets from MSigDB. We observed that the single cell hallmark

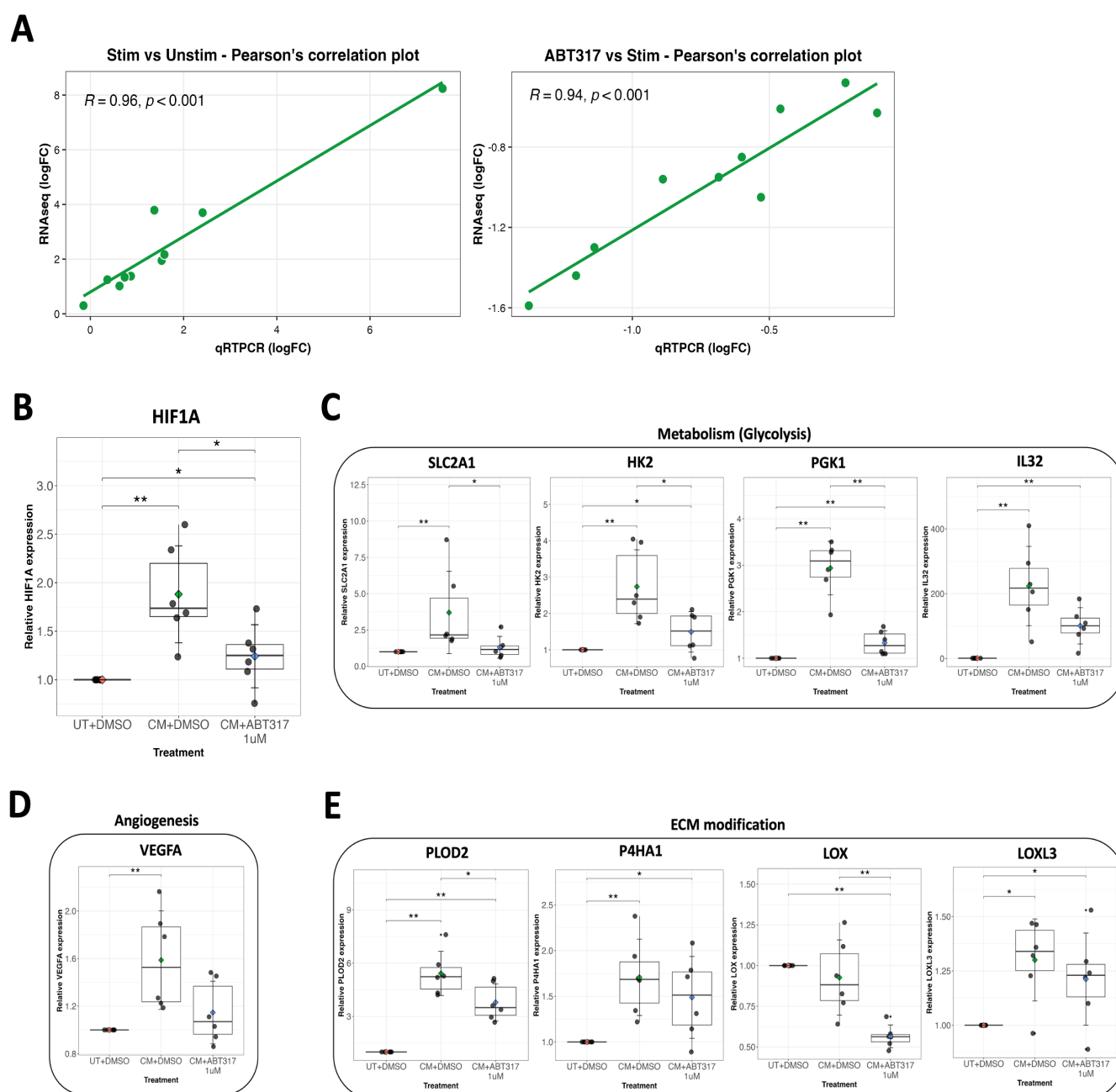


**Fig. 3.** Real-time quantitative PCR (qRT-PCR) validation of RNA seq data.

**A:** Correlation plots for comparing qRT-PCR and RNA sequencing data. Pearson's correlation coefficient values ( $R$ ) were calculated with  $p$ -values between qRT-PCR and RNAseq data using log2 fold change (logFC) results.

**B:** qRT-PCR validation for the expression of hypoxia marker HIF1A in response to CM-stimulation (Stim) and ABT-317 1 $\mu$ M (Stim). Relative expression values were generated for qRT-PCR samples by comparing the expression of genes at each treatment using the  $2^{-\Delta\Delta Ct}$  method. Data are presented as means  $\pm$  standard error (SE) from six independent biological replicates and two technical replicates.

$p$  adjusted value was calculated by Wilcoxon Rank Sum test. \* $p < 0.05$ , \*\* $p < 0.005$ .

**C:** qRT-PCR validation for the expression of glycolysis related genes in response to CM-stimulation (Stim) and ABT-317 1 $\mu$ M (Stim). Relative expression values were generated for qRT-PCR samples by comparing the expression of genes at each treatment using the  $2^{-\Delta\Delta Ct}$  method. Data are presented as means  $\pm$  standard error (SE) from six independent biological replicates and two technical replicates.

$p$  adjusted value was calculated by Wilcoxon Rank Sum test. \* $p < 0.05$ , \*\* $p < 0.005$ .

**D:** qRT-PCR validation for the expression of angiogenesis marker VEGFA in response to CM-stimulation (Stim) and ABT-317 1 $\mu$ M (Stim). Relative expression values were generated for qRT-PCR samples by comparing the expression of genes at each treatment using the  $2^{-\Delta\Delta Ct}$  method. Data are presented as means  $\pm$  standard error (SE) from six independent biological replicates and two technical replicates.

$p$  adjusted value was calculated by Wilcoxon Rank Sum test. \*\* $p < 0.005$ .

**E:** qRT-PCR validation for the expression of extracellular matrix genes in response to CM-stimulation (Stim) and ABT-317 1 $\mu$ M (Stim). Relative expression values were generated for qRT-PCR samples by comparing the expression of genes at each treatment using the  $2^{-\Delta\Delta Ct}$  method. Data are presented as means  $\pm$  standard error (SE) from six independent biological replicates and two technical replicates.

$p$  adjusted value was calculated by Wilcoxon Rank Sum test. \*\* $p < 0.005$ .

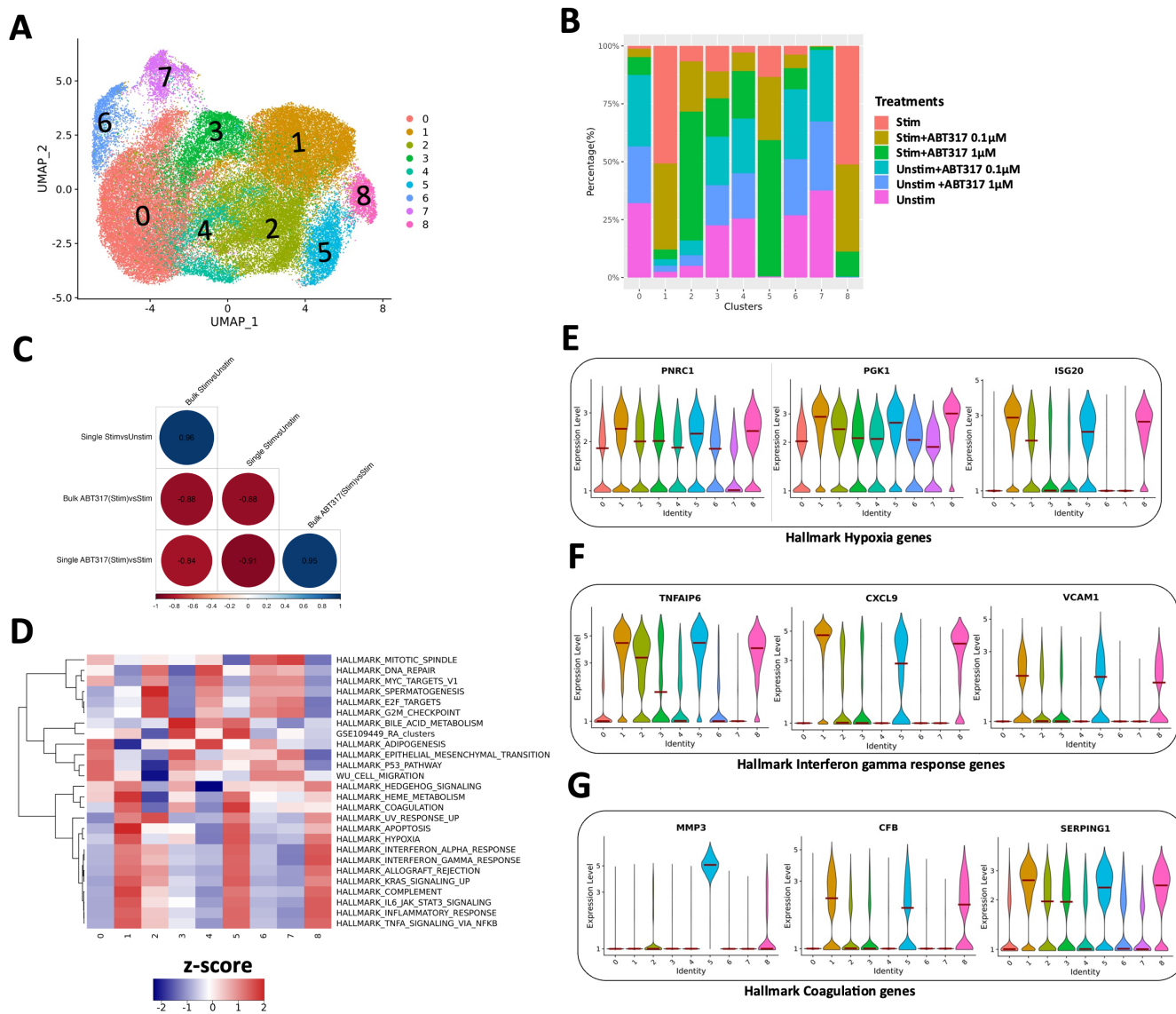


**Fig. 4.** Heterogeneous cell status of RA-FLS cells in conditioned media and ABT-317. **A:** UMAP plots of all 87,108 cells by Seurat clustering. Clusters were identified using Seurat’s FindClusters function with a resolution = 0.2. **B:** Stacked bar plot showing the percentage of cells from each treatment present in the Seurat clusters with the summary of clusters. **C:** Correlation heatmap plots for DEGs between single cell RNAseq and bulk RNAseq. Pearson’s correlation coefficient values (R) between the single and bulk RNAseq DEGs analysis results were calculated. Insignificant ( $p > 0.05$ ) value is marked as a cross (X). **D:** Heatmap plot for hallmark gene set signatures in Seurat clusters. Hallmark gene set signatures were selected from bulk RNAseq data in Fig. 2A and B. Colour scale indicates relative GSEA scores (Z-score). Hallmark enrichment scores and False discovery rate (FDR) are calculated with the singleseqset R package (47) and plotted with a threshold of FDR <10%. **E:** Violin plots for differentially expressed genes from Hallmark hypoxia signature between clusters 2 and 5. Red bar depicts the median gene expression levels in each cluster. **F:** Violin plots for differentially expressed genes from Hallmark interferon gamma response signature between clusters 2 and 5. Red bar depicts the median gene expression levels in each cluster. **G:** Violin plots for differentially expressed genes from Hallmark coagulation signature between clusters 2 and 5. Red bar depicts the median gene expression levels in each cluster.

GSEA results were similar to our bulk RNAseq GSEA data between CM-stimulation and ABT-317 (Stim) (Fig. 2A and Fig. 4D). For example, clusters 1 and 8 (Stim-driven clusters) have the highest enrichment score for inflammatory signalling and hypoxia related hallmark gene signatures, while cluster 2 (ABT-317 driven cluster in CM-

stim) shows lower scores than cluster 1. Surprisingly, we found heterogeneous Hallmark GSEA signatures in clusters 2 and 5 although both clusters are mainly driven by ABT-317 treatment in CM-stimulation (Fig. 4B). We have also observed that many RA pathogenesis related genes were elevated in cluster 5 compared to cluster 2. For example, hy-

poxia related genes like PNRC1, PGK1, and ISG20 were highly expressed in cluster 5 while cluster 2 showed lower gene expression levels for these genes (Fig. 4E). We also observed that interferon gamma response genes such as TNFAIP6, CXCL9, and VCAM1 were heterogeneously expressed in each cluster (Fig. 4F). Interestingly, VCAM1 is

known to be expressed in activated synovial fibroblasts, and it is thought to be involved in the pathogenesis of inflammatory joint diseases (29), suggesting that clusters 1, 5, and 8 may be related to an activated synovial fibroblast phenotype. Coagulation related genes like MMP3, CFB, and SERPING1 were highly expressed in cluster 5 while cluster 2 showed relatively lower expression levels of these genes (Fig. 4G). In particular, MMP3 was the top marker gene in cluster 5 and is known to be involved in the pathogenesis of rheumatoid arthritis (30, 31). Taken together, our results suggest that cells within cluster 5 have features resembling those that are strongly associated with rheumatoid arthritis pathogenesis including hypoxia, interferon gamma response, and coagulation pathways and while decreased overall by ABT-317, specific RA-FLS cells may be resistant to JAK inhibition, be a result of incomplete inhibition, or be driven by JAK independent mechanisms, leading to heterogenous populations of RA-FLS.

## Discussion

In this study, we exploited bulk and single cell RNA sequencing to capture the JAK1 inhibitor effects on RA synovial fibroblasts. Our approach successfully captured the transcriptomic changes in RA-FLS after stimulating with conditioned media as well as treating with a JAK1 selective inhibitor (ABT-317). Gene set enrichment analysis (GSEA) demonstrated that the JAK1 inhibitor reduced not only the expected inflammatory pathways like interferon and IL-6 signalling but also in reduced non-inflammatory pathways, such as hypoxia and cell migration. Notably, our bulk RNA-seq data significantly correlates with that of publicly available RA tissue microarray data sets, supporting the use of CM-stimulation as an *in vitro* model system to study RA-FLS pathogenic responses. Single cell RNA-seq analysis of CM-activated cultured RA-FLS confirmed decreases in inflammatory and non-inflammatory pathways with JAK inhibition, but also identified a heterogenous cell status that reflects differential inhibition of pathogenic pathways at the single cell level.

Our GSEA results from CM-stimulation successfully captured the upregulated JAK-STAT pathways and were down regulated upon JAK inhibitor treatment. Different JAK-specific inhibitors selectively suppress different types of STATs which specifically regulate their own molecular targets in synovial fibroblasts. For example, while peficitinib (pan-JAKi) and tofacitinib (JAK1,3 less JAK2 selective inhibitor) decrease the protein levels of pSTAT3 (32), PF-956980 (JAK3 selective inhibitor) did not affect STAT3 activation but it suppressed STAT1 and STAT5 activation in Oncostatin M (OSM)-stimulated RA-FLS (33). In our study, ABT-317 (JAK1 selective inhibitor) reduced the expression levels of STAT2, 3, and 5. Although we did not observe significant changes of STAT1 expression levels by our JAK1 selective inhibitor, we found B-cell activating factor/tumour necrosis factor superfamily member 13B (BAFF) was significantly reduced. Tofacitinib was reported to suppress the TNF-induced pSTAT1 and the associated inflammatory interferon response genes like BAFF in synovial fibroblasts (4) suggesting that our ABT-317 may decrease the protein levels or the signalling through STAT1 in RA-FLS. One of our interesting findings was that JAK inhibition affects additional molecular mechanisms in synovial fibroblasts beyond pro-inflammatory signalling. In particular, RA synovial fibroblasts can activate glycolytic metabolism under pro-inflammatory and hypoxic condition (4) and the increased glycolytic metabolism induced the release of IL-1 $\beta$  from macrophages (34). Consequently, the upregulated glycolytic enzymes can lead to increased amounts of lactate and succinate (4, 34) and the synovial tissue is enriched with HIF-1, a critical hypoxia associated transcriptional regulator (35). HIF-1 contributes to RA pathogenesis by promoting extracellular matrix (ECM) remodelling, which involves changes in cell morphology, adhesion, and invasion (36). In this study, we found that CM-stimulation increases HIF1A and subsequent glycolytic signals, and the expression levels of these genes are decreased following JAK1 selective

inhibitor (ABT-317) treatment. This is consistent with the previous study with tofacitinib showing that tofacitinib (1,000 nM) decreased pro-inflammatory and pro-glycolytic mediators in synovial fibroblasts from RA patients (37). Our findings suggest that HIF-1 mediated ECM remodelling by fibroblasts can be altered by the JAK1 selective inhibitor (ABT-317) during CM-stimulation. The reduction of gene enrichment score from WU-cell migration also supports the impact of ABT-317 on the ECM remodelling process.

While our data indicated that the JAK1 inhibitor mainly showed the inhibitory effects on RA-FLS, we also observed that the JAK1 inhibitor (ABT-317) reversed the CM-stimulation effects of reducing cell cycle related pathways. This result is consistent with the cell cytotoxicity test since we also observed slightly decreased cell viability in the CM-stimulation group, whereas ABT-317 slightly increased cell viability (Suppl. Fig. S1). These were unexpected findings given that most JAK inhibitors have been shown to induce cell cycle arrest in cancer cells (38, 39), but could be related to the inflammatory stimuli used in these studies and/or the reversing effects of JAK inhibitors on inflammatory processes.

The observation of unique populations of fibroblasts emerging upon activation and JAK1 inhibitor treatment is consistent with a previous report of the heterogenous cell status in response to cytokine signalling in cultured synovial fibroblasts (40). Of the several different clusters that emerged with CM and JAK inhibitor treatment, we identified a PRG4<sup>hi</sup> cluster (cluster 4) that might represent cells of the synovial lining (41) and it suggests that the cellular heterogeneity can be induced in cultured fibroblast cells, which normally become homogenous upon removal from the *in vivo* setting and cultured on 2 dimensional plastic. Notably, we found the presence of heterogenous cell populations driven from the JAK1 inhibitor treatment. Although MMP3<sup>hi</sup> cluster (cluster 5) and cluster 2 are mainly driven from the JAK1 inhibitor with CM-stimulation, MMP3<sup>hi</sup> cluster did not show the reduced gene signa-

tures of interferon gamma response signalling, hypoxia, and coagulation compared to CM-stimulation driven clusters. This may indicate an incomplete inhibitory effect of the JAK1 inhibitor, an intrinsic resistance of certain cells to JAK1 inhibition or are driven by JAK-independent mechanisms.

The cluster that appeared to retain pathogenic properties was cluster 5 (MMP3<sup>hi</sup>) and express high levels of CXCL1 and CXCL8 genes. It has been shown that multiple JAK inhibitors do not strongly reduce the protein levels of CXCL8, CXCL1, and MMP3 in IL-1 $\beta$ -stimulated RA synovial fibroblasts (42). MMPs are mainly induced by IL-1 $\beta$  in the elevated glycolytic metabolism (34) and have been implicated in FLS invasiveness (40, 43). Additionally, a recent study of inflammatory bowel disease has shown that IL-1 $\beta$ -activated fibroblast signature in certain pathotypes may be associated with the low response rates to multiple therapies (44). Collectively, these data suggests that cluster 5 (MMP3<sup>hi</sup>) could be driven by IL-1 $\beta$ -induced responses, which are JAK independent.

This unique cluster 5 (MMP3<sup>hi</sup>) also showed higher gene expressions of transporter genes like SERPINA1 or SLC2A5 than the other JAK inhibitor-driven cluster (cluster 2, Suppl. Table S6). This may explain the distinct features of two JAKi driven clusters, since transporters are known to be involved in multidrug resistance in cancer cells (45, 46) and could reflect a resistance of this subpopulation to the inhibitor. Interestingly, a previous study has shown that the secretion of MMP3 is not efficiently suppressed by different JAK inhibitors in stimulated FLS cultures while a potent suppression of MMP3 secretion was achieved by treating FLS with adalimumab (anti-TNF- $\alpha$ ), secukinumab (anti-IL-17A), and canakinumab (anti-IL-1 $\beta$ ) (47). This suggests that combining therapies that can address other fibroblast functions with JAK inhibitors may provide additive effects to treat drug-resistant RA-FLS.

Our study in RA-FLS cells has revealed how the JAK1 selective inhibitor, ABT-317, can significantly alter the transcriptomic landscape and gene sig-

natures of these cells, especially under a pro-inflammatory condition such as that observed with CM-stimulation. By using a single cell RNAseq approach, we have also found that CM-stimulation and the JAK1 inhibitor treatment of RA-FLS can induce heterogenous cell status changes in these cells. The limitations of *in vitro* RA-FLS models include that they may not fully represent the complex RA synovium microenvironment in RA patient although we have shown the significant correlation of our data with the public RA tissue microarray dataset. This will necessitate further research and the development of relevant RA biology model using 3D-cell culture or organoid models. Overall, our study provides an important advance in the understanding of the JAK1 inhibitor's molecular mechanisms on RA-FLS and serves as an essential resource for future in-depth research in identifying molecular responses of JAK inhibitors on RA-FLS cells.

#### Acknowledgments

We would like to thank Lori Dowding from AbbVie for assistance with qRT-PCR. We would like to thank Timothy Radstake and Dan Chang from AbbVie for their invaluable assistance with review of the manuscript.

#### References

- HARRE U, SCHETT G: Cellular and molecular pathways of structural damage in rheumatoid arthritis. *Semin Immunopathol* 2017; 39(4): 355-63. <http://doi.org/10.1007/s00281-017-0634-0>
- CHU CQ: Highlights of strategies targeting fibroblasts for novel therapies for rheumatoid arthritis. *Front Med* 2022; 9: 846300. <http://doi.org/10.3389/fmed.2022.846300>
- OWEN KL, BROCKWELL NK, PARKER BS: JAK-STAT Signaling: a double-edged sword of immune regulation and cancer progression. *Cancers* 2019; 11(12): 2002. <http://doi.org/10.3390/cancers11122002>
- BURJA B, MERTELJ T, FRANK-BERTONCELJ M: Hi-JAKi-ng synovial fibroblasts in inflammatory arthritis with JAK inhibitors. *Front Med* 2020; 7: 124. <http://doi.org/10.3389/fmed.2020.00124>
- HODGE JA, KAWABATA TT, KRISHNASWAMI S *et al.*: The mechanism of action of tofacitinib - an oral Janus kinase inhibitor for the treatment of rheumatoid arthritis. *Clin Exp Rheumatol* 2015; 34(2): 318-28.
- BARTOK B, FIRESTEIN GS: Fibroblast-like synoviocytes: key effector cells in rheumatoid arthritis. *Immunol Rev* 2010; 233(1): 233-55. <http://doi.org/10.1111/j.0105-2896.2009.00859.x>

- NYGAARD G, FIRESTEIN GS: Restoring synovial homeostasis in rheumatoid arthritis by targeting fibroblast-like synoviocytes. *Nat Rev Rheumatol* 2020; 16(6): 316-33. <http://doi.org/10.1038/s41584-020-0413-5>
- ZHANG F, JONSSON AH, NATHAN A *et al.*: Cellular deconstruction of inflamed synovium defines diverse inflammatory phenotypes in rheumatoid arthritis. *bioRxiv*. Published online 2022: 2022.02.25.481990. <http://doi.org/10.1101/2022.02.25.481990>
- ZHANG F, WEI K, SLOWIKOWSKI K *et al.*: Defining inflammatory cell states in rheumatoid arthritis joint synovial tissues by integrating single-cell transcriptomics and mass cytometry. *Nat Immunol* 2019; 20(7): 928-42. <http://doi.org/10.1038/s41590-019-0378-1>
- MIZOGUCHI F, SLOWIKOWSKI K, WEI K *et al.*: Functionally distinct disease-associated fibroblast subsets in rheumatoid arthritis. *Nat Commun* 2018; 9(1): 789. <http://doi.org/10.1038/s41467-018-02892-y>
- GE T, JHALA G, FYNCH S *et al.*: The JAK1 Selective inhibitor ABT 317 blocks signaling through interferon- $\gamma$  and common  $\gamma$  chain cytokine receptors to reverse autoimmune diabetes in NOD mice. *Front Immunol* 2020; 11: 588543. <http://doi.org/10.3389/fimmu.2020.588543>
- KRAKAUER T: Update on staphylococcal superantigen-induced signaling pathways and therapeutic interventions. *Toxins* 2013; 5(9): 1629-54. <http://doi.org/10.3390/toxins5091629>
- RISSO D, NGAI J, SPEED TP, DUDOIT S: Normalization of RNA-seq data using factor analysis of control genes or samples. *Nat Biotechnol* 2014; 32(9): 896-902. <http://doi.org/10.1038/nbt.2931>
- HUBER R, HUMMERT C, GAUSMANN U *et al.*: Identification of intra-group, inter-individual, and gene-specific variances in mRNA expression profiles in the rheumatoid arthritis synovial membrane. *Arthritis Res Ther* 2008; 10(4): R98-R98. <http://doi.org/10.1186/ar2485>
- WOETZEL D, HUBER R, KUPFER P *et al.*: Identification of rheumatoid arthritis and osteoarthritis patients by transcriptome-based rule set generation. *Arthritis Res Ther* 2014; 16(2): R84-R84. <http://doi.org/10.1186/ar4526>
- STUART T, BUTLER A, HOFFMAN P *et al.*: Comprehensive integration of single-cell data. *Cell* 2019; 177(7): 1888-902.e21. <http://doi.org/10.1016/j.cell.2019.05.031>
- HAFEMEISTER C, SATIJA R: Normalization and variance stabilization of single-cell RNA-seq data using regularized negative binomial regression. *Genome Biol* 2019; 20(1): 296. <http://doi.org/10.1186/s13059-019-1874-1>
- CILLO AR, KÜRTEHL CHL, TABIB T *et al.*: Immune landscape of viral- and carcinogen-driven head and neck cancer. *Immunity* 2020; 52(1): 183-99.e9. <http://doi.org/10.1016/j.immuni.2019.11.014>
- GIANNONI E, BIANCHINI F, CALORINI L, CHIARUGI P: Cancer associated fibroblasts exploit reactive oxygen species through a proinflammatory signature leading to epithe-

- lial mesenchymal transition and stemness. *Antioxid Redox Signal* 2011; 14(12): 2361-71. <http://doi.org/10.1089/ars.2010.3727>
20. TABATA Y, YOSHINO D, FUNAMOTO K, KOENS R, KAMM RD, FUNAMOTO K: Migration of vascular endothelial cells in monolayers under hypoxic exposure. *Integr Biol* 2019; 11(1): 26-35. <http://doi.org/10.1093/intbio/zyz002>
  21. DJAGAIEVA I, DORONKIN S: Hypoxia response pathway in border cell migration. *Cell Adhes Migr* 2010; 4(3): 391-95. <http://doi.org/10.4161/cam.4.3.11790>
  22. YANG N, CAO DF, YIN XX, ZHOU HH, MAO XY: Lysyl oxidases: Emerging biomarkers and therapeutic targets for various diseases. *Biomed Pharmacother* 2020; 131: 110791. <http://doi.org/10.1016/j.biopha.2020.110791>
  23. OLIVEIRA PG DE, FARINON M, SANCHEZ-LOPEZ E, MIYAMOTO S, GUMA M: Fibroblast-like synoviocytes glucose metabolism as a therapeutic target in rheumatoid arthritis. *Front Immunol* 2019; 10: 1743. <http://doi.org/10.3389/fimmu.2019.01743>
  24. ZHANG Y, CAI H, LIAO Y, ZHU Y, WANG F, HOU J: Activation of PGK1 under hypoxic conditions promotes glycolysis and increases stem cell-like properties and the epithelial-mesenchymal transition in oral squamous cell carcinoma cells via the AKT signalling pathway. *Int J Oncol* 2020; 57(3): 743-55. <http://doi.org/10.3892/ijo.2020.5083>
  25. HUANG J, YANG M, LIU Z *et al.*: PPFIA4 promotes colon cancer cell proliferation and migration by enhancing tumor glycolysis. *Front Oncol* 2021; 11: 653200. <http://doi.org/10.3389/fonc.2021.653200>
  26. QUIÑONEZ-FLORES CM, GONZÁLEZ-CHÁVEZ SA, PACHECO-TENA C: Hypoxia and its implications in rheumatoid arthritis. *J Biomed Sci* 2016; 23(1): 62. <http://doi.org/10.1186/s12929-016-0281-0>
  27. LI GQ, ZHANG Y, LIU D *et al.*: PI3 kinase/Akt/HIF-1 $\alpha$  pathway is associated with hypoxia-induced epithelial-mesenchymal transition in fibroblast-like synoviocytes of rheumatoid arthritis. *Mol Cell Biochem* 2013; 372(1-2): 221-31. <http://doi.org/10.1007/s11010-012-1463-z>
  28. PARK JS, LEE S, JEONG AL *et al.*: Hypoxia-induced IL-32 $\beta$  increases glycolysis in breast cancer cells. *Cancer Lett* 2015; 356(2): 800-8. <http://doi.org/10.1016/j.canlet.2014.10.030>
  29. CARTER WICKS IP: Vascular cell adhesion molecule 1 (CD106): A multifaceted regulator of joint inflammation. *Arthritis Rheum* 2001; 44(5): 985-94. [http://doi.org/10.1002/1529-0131\(200105\)44:5<985::aid-anr176>3.0.co;2-p](http://doi.org/10.1002/1529-0131(200105)44:5<985::aid-anr176>3.0.co;2-p)
  30. ZHAI T, GAO C, HUO R *et al.*: Cyr61 participates in the pathogenesis of rheumatoid arthritis via promoting MMP-3 expression by fibroblast-like synoviocytes. *Mod Rheumatol* 2017; 27(3): 466-75. <http://doi.org/10.1080/14397595.2016.1220447>
  31. SUN S, BAY-JENSEN AC, KARSDAL MA *et al.*: The active form of MMP-3 is a marker of synovial inflammation and cartilage turnover in inflammatory joint diseases. *BMC Musculoskelet Disord* 2014; 15(1): 93-93. <http://doi.org/10.1186/1471-2474-15-93>
  32. EMORI T, KASAHARA M, SUGAHARA S *et al.*: Role of JAK-STAT signaling in the pathogenic behavior of fibroblast-like synoviocytes in rheumatoid arthritis: Effect of the novel JAK inhibitor peficitinib. *Eur J Pharmacol* 2020; 882: 173238. <http://doi.org/10.1016/j.ejphar.2020.173238>
  33. MIGITA K, IZUMI Y, TORIGOSHI T *et al.*: Inhibition of Janus kinase/signal transducer and activator of transcription (JAK/STAT) signalling pathway in rheumatoid synovial fibroblasts using small molecule compounds. *Clin Exp Immunol* 2013; 174(3): 356-63. <http://doi.org/10.1111/cei.12190>
  34. LITTLEWOOD-EVANS A, SARRET S, APFEL V *et al.*: GPR91 senses extracellular succinate released from inflammatory macrophages and exacerbates rheumatoid arthritis. *J Exp Med* 2016; 213(9): 1655-62. <http://doi.org/10.1084/jem.20160061>
  35. IOMMARINI L, PORCELLI AM, GASPARRE G, KURELAC I: Non-canonical mechanisms regulating hypoxia-inducible factor 1 alpha in cancer. *Front Oncol* 2017; 7: 286. <http://doi.org/10.3389/fonc.2017.00286>
  36. PETROVA V, ANNICCHIARICO-PETRUZZELLI M, MELINO G, AMELIO I: The hypoxic tumour microenvironment. *Oncogenesis* 2018; 7(1): 10. <http://doi.org/10.1038/s41389-017-0011-9>
  37. MCGARRY T, ORR C, WADE S *et al.*: JAK/STAT blockade alters synovial bioenergetics, mitochondrial function, and proinflammatory mediators in rheumatoid arthritis. *Arthritis Rheumatol* 2018; 70(12): 1959-70. <http://doi.org/10.1002/art.40569>
  38. SHE S, ZHAO Y, KANG B *et al.*: Combined inhibition of JAK1/2 and DNMT1 by newly identified small-molecule compounds synergistically suppresses the survival and proliferation of cervical cancer cells. *Cell Death Dis* 2020; 11(9): 724. <http://doi.org/10.1038/s41419-020-02934-8>
  39. FUKE H, SHIRAKI K, SUGIMOTO K *et al.*: JAK inhibitor induces S phase cell-cycle arrest and augments TRAIL-induced apoptosis in human hepatocellular carcinoma cells. *Biochem Biophys Res Commun* 2007; 363(3): 738-44. <http://doi.org/10.1016/j.bbrc.2007.09.049>
  40. SMITH MH, GAO VR, PERIYAKOIL PK *et al.*: Drivers of heterogeneity in synovial fibroblasts in rheumatoid arthritis. *Nat Immunol* 2023; 24(7): 1200-10. <http://doi.org/10.1038/s41590-023-01527-9>
  41. RHEE DK, MARCELINO J, BAKER M *et al.*: The secreted glycoprotein lubricin protects cartilage surfaces and inhibits synovial cell overgrowth. *J Clin Invest* 2005; 115(3): 622-31. <http://doi.org/10.1172/jci22263>
  42. DILLER M, HASSELI R, HÜLSER ML *et al.*: Targeting activated synovial fibroblasts in rheumatoid arthritis by peficitinib. *Front Immunol* 2019; 10: 541. <http://doi.org/10.3389/fimmu.2019.00541>
  43. TOLBOOM TCA, PIETERMAN E, VAN DER LAAN WH *et al.*: Invasive properties of fibroblast-like synoviocytes: correlation with growth characteristics and expression of MMP-1, MMP-3, and MMP-10. *Ann Rheum Dis* 2002; 61(11): 975. <http://doi.org/10.1136/ard.61.11.975>
  44. FRIEDRICH M, POHIN M, JACKSON MA *et al.*: IL-1-driven stromal-neutrophil interactions define a subset of patients with inflammatory bowel disease that does not respond to therapies. *Nat Med* 2021; 27(11): 1970-81. <http://doi.org/10.1038/s41591-021-01520-5>
  45. SHEN Y, YAN Z: Systematic prediction of drug resistance caused by transporter genes in cancer cells. *Sci Rep* 2021; 11(1): 7400. <http://doi.org/10.1038/s41598-021-86921-9>
  46. ZHAO P, HUANG J, ZHANG D *et al.*: SLC2A5 overexpression in childhood Philadelphia chromosome-positive acute lymphoblastic leukaemia. *Br J Haematol* 2018; 183(2): 242-50. <http://doi.org/10.1111/bjh.15580>
  47. YAO N, TRETTER T, KVACSKAY P *et al.*: Targeting of Janus Kinases limits pro-inflammatory but also immunosuppressive circuits in the crosstalk between synovial fibroblasts and lymphocytes. *Biomedicines* 2021; 9(10): 1413. <http://doi.org/10.3390/biomedicines9101413>